TRIPLE-PASS-BAND, DUAL-STOP-BAND UWB ANTENNA WITH SUBSTRATE-INTEGRATED WAVEGUIDE RESONATORS

Qianqian Wang and Jens Bornemann
Department of Electrical and Computer Engineering, University of Victoria, Victoria, BC V8W 2Y2, Canada; Corresponding author: j.bornemann@ieee.org

Received 12 September 2013

ABSTRACT: *A coplanar-waveguide fed ultra-wideband (UWB) antenna with substrate-integrated waveguide (SIW) stop-band resonators is introduced for the 3–10 GHz band. The symmetrically placed SIW cavities provide dual-stop-band characteristics due to their TE_{101} and TE_{102} resonance modes. Thus, the entire UWB is divided into three pass-bands which cover the frequency ranges 4.23–4.62 GHz, 6.6–8.175 GHz, and 9.39–10.7 GHz. Measurements of a prototype show good agreement with simulation results with a minimum measured return loss of 9 dB in any of the three pass-bands.* © 2014 Wiley Periodicals, Inc. Microwave Opt Technol Lett 56:1265–1270, 2014; View this article online at wileyonlinelibrary.com. DOI 10.1002/mop.28320

Key words: *ultra-wideband antennas; coplanar waveguide; substrate-integrated waveguide; stop-band filter*

1. INTRODUCTION

With the release of the 3.1–10.6 GHz band for ultra-wideband (UWB) communication, a number of diverse applications have been proposed and implemented such as systems related to imaging, medical monitoring, surveillance, ground penetrating and vehicular radar, communications, measurements and many more. Portable handhelds for short-range and large bandwidth communications will be required in future UWB systems. Thus, there is a demand for the implementation of UWB antennas in printed-circuit technologies.

Over the last decade, a variety of printed-circuit UWB antennas have been proposed. They use either microstrip, for example, [1–4] or coplanar-waveguide (CPW) technologies, for example, [4–7]. Although CPW has the advantage of requiring fabrication on only a single side of the substrate, microstrip is more versatile as antenna elements may be printed on both substrate sides [8].

To avoid interference with existing wireless networks, UWB antennas are in need of band-rejection capabilities. Instead of adding new circuits to the communication system, stop-band techniques can be applied directly to the UWB planar antenna, for example, [9–12]. However, common practice is to realize the integration of notch circuits with microstrip or slot-line resonators. Their relatively low quality factor usually results in broadband notches with low attenuation and mediocre selectivity [13].

Therefore, this article introduces substrate-integrated waveguide (SIW) resonators to improve the selectivity of stop-bands in UWB antennas because Q factors of SIW cavities are an order of magnitude higher than those of microstrip resonators [14]. A similar approach is presented in Ref. 15 for the 1–7 GHz band where a microstrip feed line is placed on top of a single SIW resonator. However, the return loss values within some of the pass-bands are only 4 dB and thus not that much different

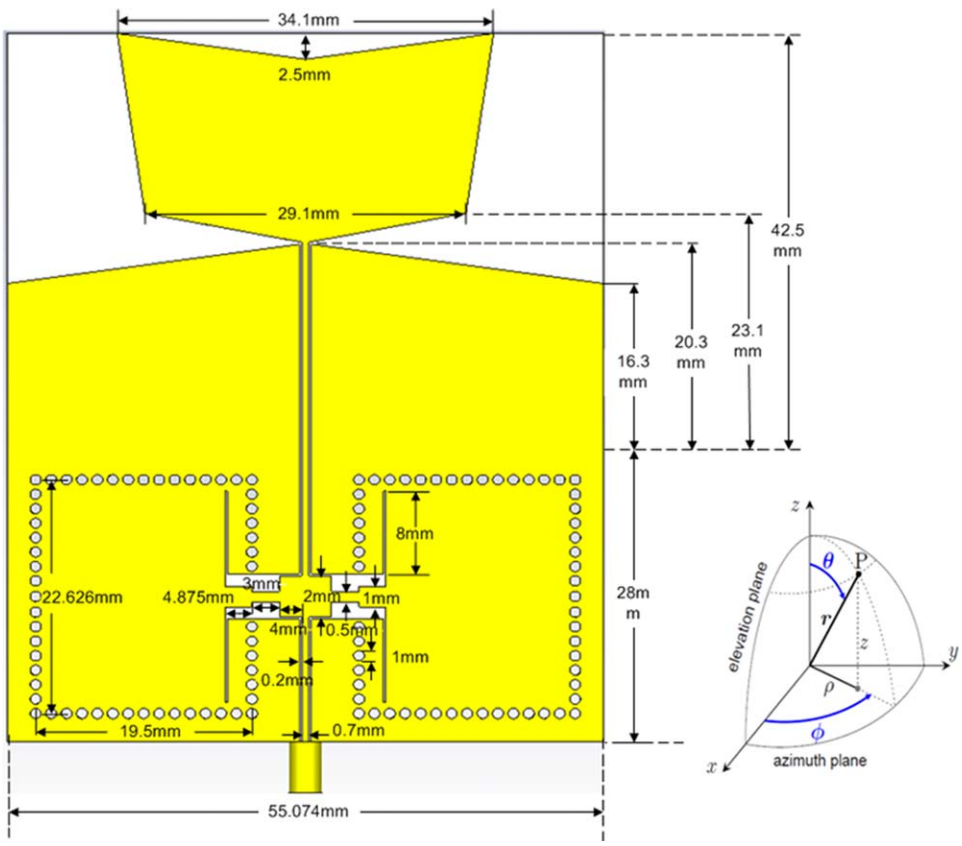

Figure 1 Schematic view of the CPW-fed UWB antenna with SIW band-stop resonators, and definition of the coordinate system for pattern plots. [Color figure can be viewed in the online issue, which is available at wileyonlinelibrary.com]

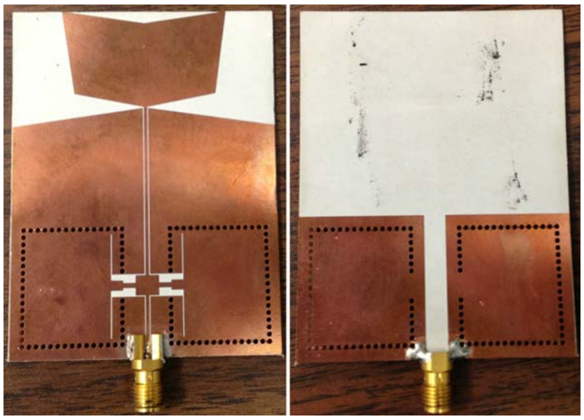

Figure 2 Photograph of the fabricated prototype: front (left) and back (right). [Color figure can be viewed in the online issue, which is available at wileyonlinelibrary.com]

from the stop-bands. This article demonstrates that pass-band return losses of close to 10 dB are possible in three different pass-bands and that the two stop-bands provide rejection in the order of 10 dB.

2. DESIGN

The design of the CPW-fed UWB antenna element is adapted from Ref. 4, where RT/Duroid 6002 substrate was used with $\varepsilon_r = 2.94$, tan $\delta = 0.0012$, substrate height $h = 508$ μm, metallization thickness $t = 17.5$ μm, and conductivity $\sigma = 5.8 \times 10^8$ S/m. Figure 1 depicts the layout of the UWB antenna with SIW band-stop resonators and outlines all dimensions as well as the coordinate system used in this work. To maintain a reasonable center conductor to slot width ratio (0.7 mm/0.2 mm), the impedance of the feeding CPW is selected as 70.8 Ω. Note that the 50 Ω coaxial connector is included in all simulations and, therefore, this impedance mismatch (VSWR = 1.4) is fully taken into account.

The band-stop filter is designed with two identical SIW resonators to maintain symmetry. For pattern symmetry and group delay performance, symmetric SIW resonators assure that the UBW antenna is fed with the fundamental (even) CPW mode as opposed to a combination of even and odd modes. According to

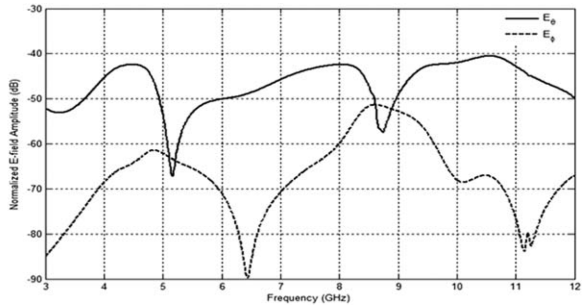

Figure 4 Simulated amplitude responses of the co- and cross-polarized electric fields with probes located at $\Theta = 90°$ and $\Phi = 90°$

design guidelines presented in Ref. 16, the equivalent waveguide width, a_{equ}, is given as

$$a_{\mathrm{equ}} = \frac{c}{2 f_c \sqrt{\varepsilon_r}} \tag{1}$$

where c is the speed of light and f_c is the cutoff frequency which is set to 4 GHz via diameter d and center-to-center spacing p are chosen according to Ref. 17, leading to $p = 1$ mm and $d = 1.4$ mm. Thus, the d/p ratio is 0.71 which is well within the recommended range between 0.5 and 0.8. After the equivalent waveguide width, $a_{\mathrm{equ}} = 21.855$ mm is obtained from (1), the actual width a of the SIW resonators is extracted from Ref. 16 and is found as $a = 22.626$ mm, compared to Figure 1. The distances between the SIW resonators to the antenna and to the coaxial feed have been determined in parametric studies which are not shown here. The same holds for the CPW-to-SIW transitions.

The guided wavelength in a SIW structure is given as

$$\lambda_g = \frac{c}{\sqrt{\varepsilon_r}\sqrt{f^2 - f_c^2}} \tag{2}$$

such that a half-wavelength resonator at 6 GHz is 19.5 mm long. The next harmonic of the resonator falls inside the band and theoretically appears at 9.8 GHz. However, due to the CPW-to-SIW transitions used to excite the resonators, the resonances shift slight downward and appear at 5.2 and 8.7 GHz. Note that unless a single stop-band is desired in the upper UWB spectrum, waveguide-based resonators will always demonstrate a second pass-band within the UWB range. However,

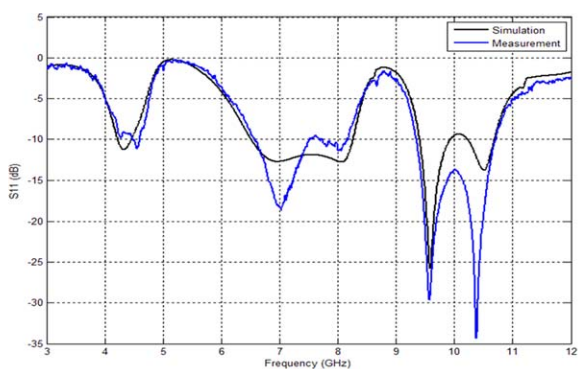

Figure 3 Reflection coefficient comparison between simulation and measurement. [Color figure can be viewed in the online issue, which is available at wileyonlinelibrary.com]

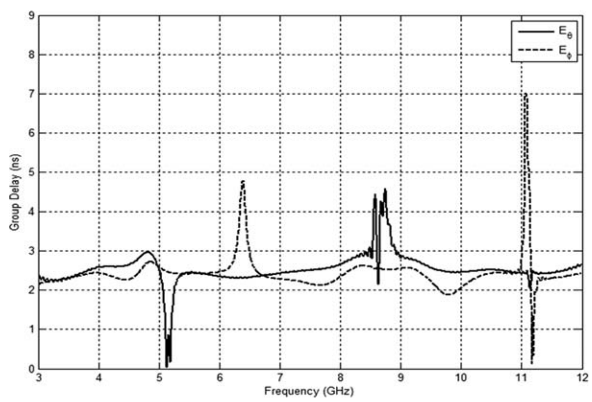

Figure 5 Simulated group delay performance of UWB antenna in Figure 1 with probes at $\Theta = 90°$ and $\Phi = 90°$

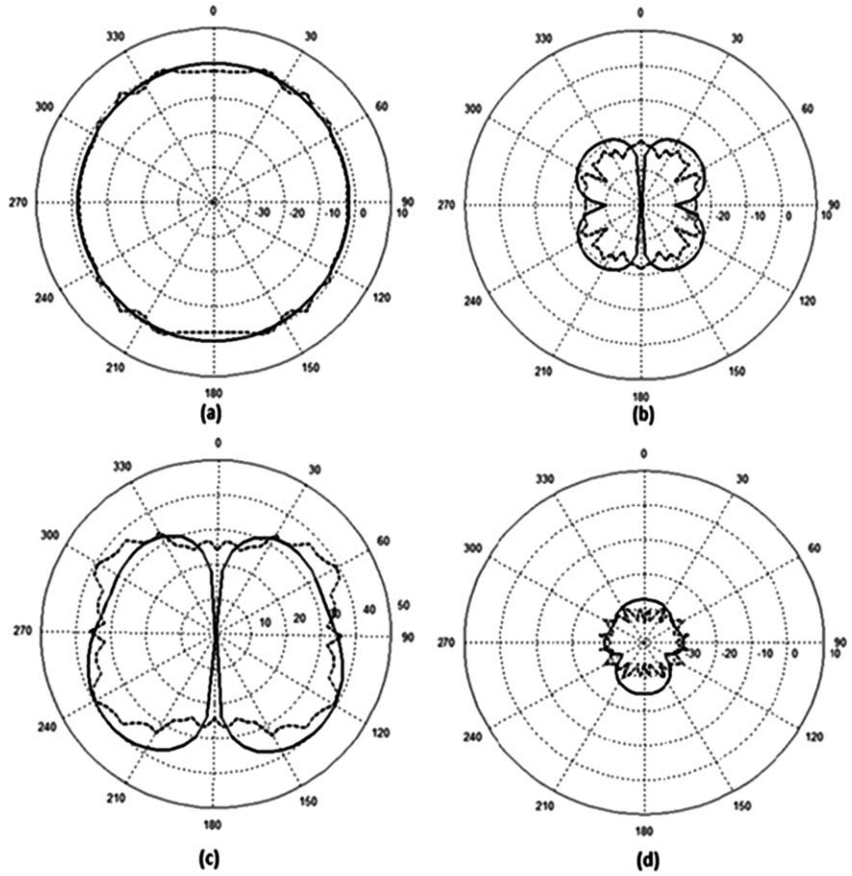

Figure 6 Normalized radiation patterns in the first pass-band at 4.3 GHz—simulated (solid line) and measurements (dotted line): (a) co-pol *H*-plane, (b) x-pol *H*-plane, (c) co-pol *E*-plane, and (d) x-pol *E*-plane

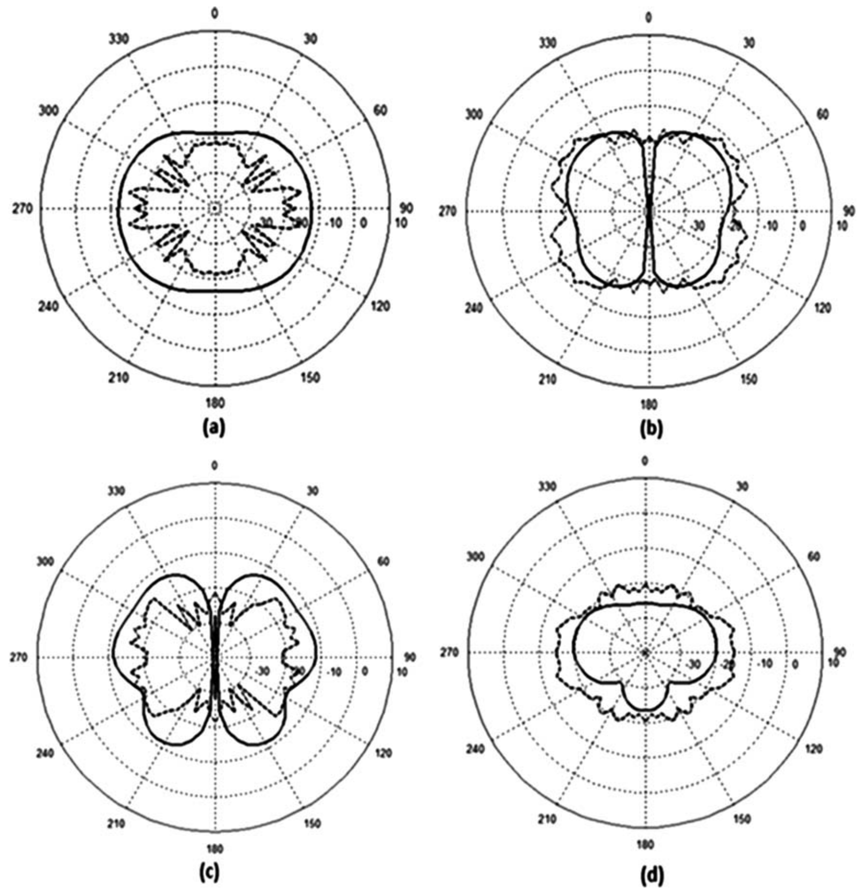

Figure 7 Normalized radiation patterns in the first stop-band at 5 GHz—simulated (solid line) and measurements (dotted line): (a) co-pol *H*-plane, (b) x-pol *H*-plane, (c) co-pol *E*-plane, and (d) x-pol *E*-plane

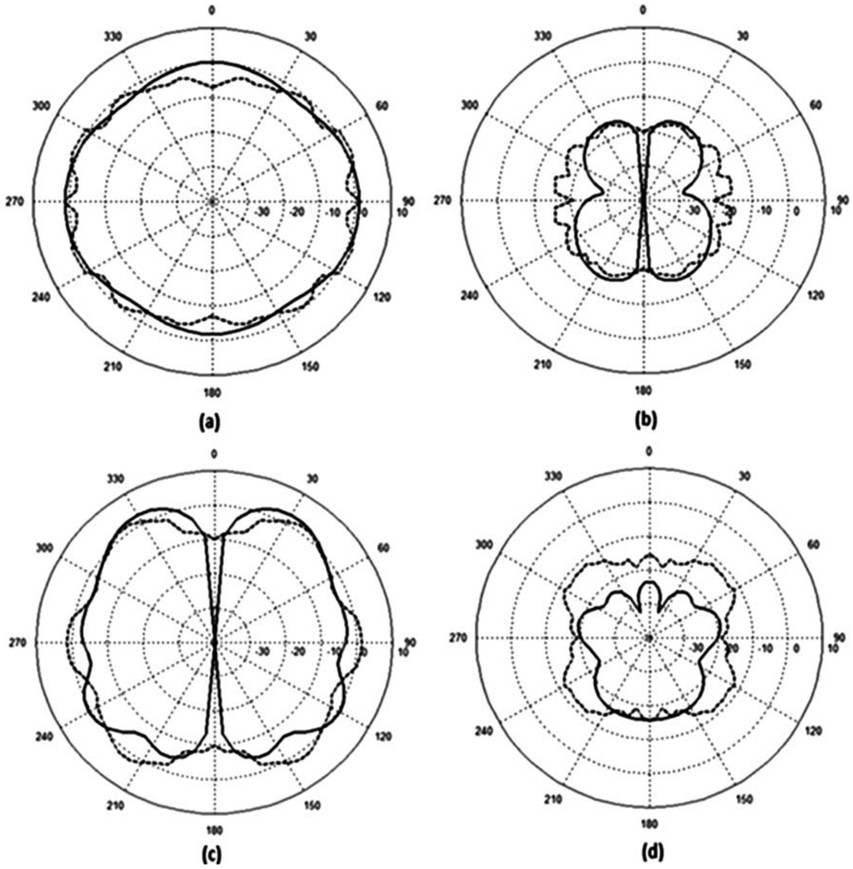

Figure 8 Normalized radiation patterns in the second pass-band at 7 GHz—simulated (solid line) and measurements (dotted line): (a) co-pol *H*-plane, (b) x-pol *H*-plane, (c) co-pol *E*-plane, and (d) x-pol *E*-plane

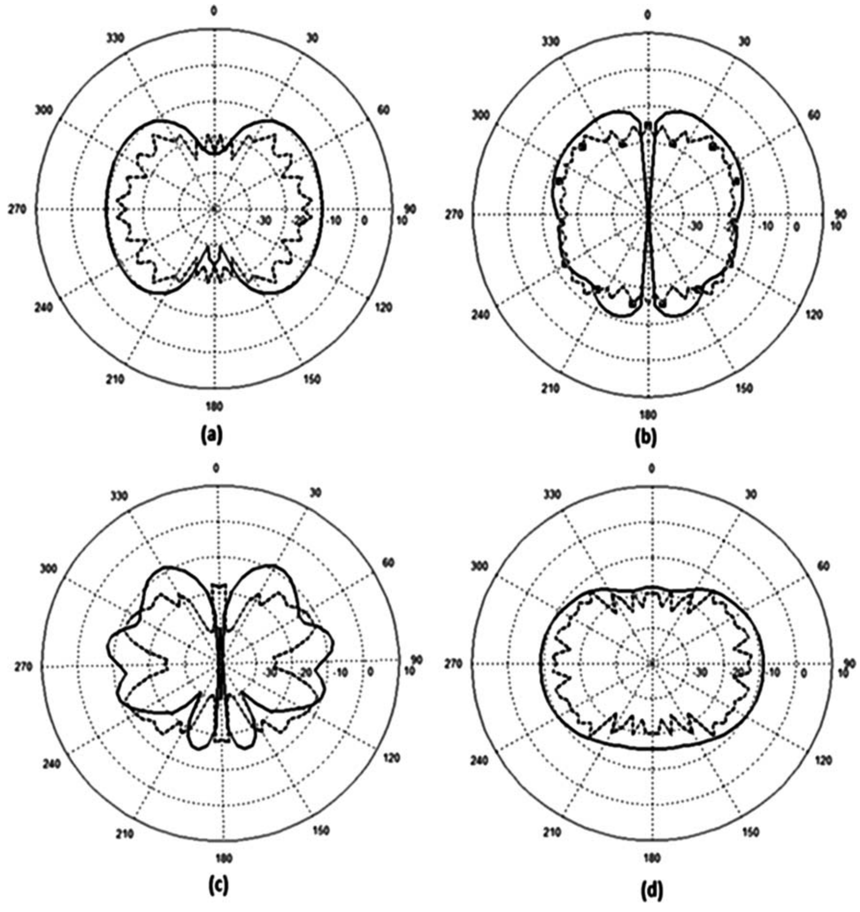

Figure 9 Normalized radiation patterns in the second stop-band at 9 GHz—simulated (solid line) and measurements (dotted line): (a) co-pol *H*-plane, (b) x-pol *H*-plane, (c) co-pol *E*-plane, and (d) x-pol *E*-plane

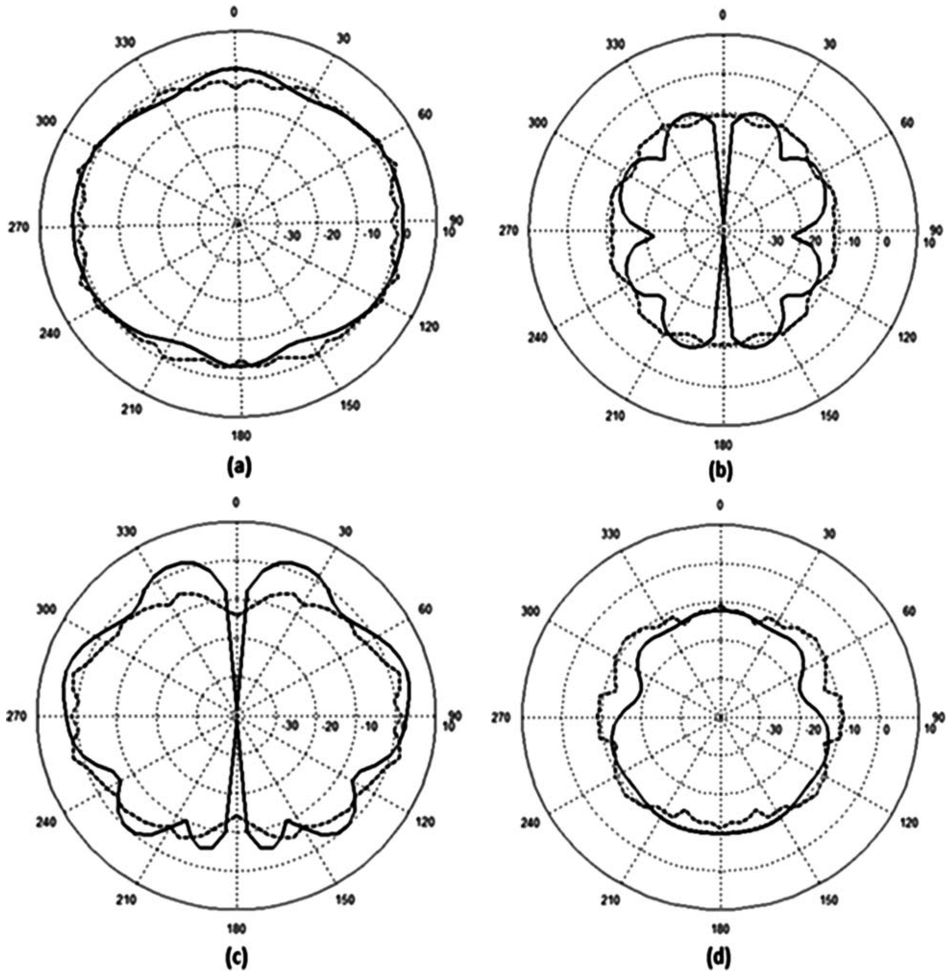

Figure 10 Normalized radiation patterns in the third pass-band at 10 GHz—simulated (solid line) and measurements (dotted line): (a) co-pol *H*-plane, (b) x-pol *H*-plane, (c) co-pol *E*-plane, and (d) x-pol *E*-plane

within limits, the position of the second stop-band can be adjusted by changing the cutoff frequency f_c of the SIW cavities. For instance, if the cutoff frequency of the SIW resonators had been chosen as 4.8 GHz instead of 4 GHz and if the first stop-band remained at 6 GHz, then the second stop-band of the SIW resonator would occur at 8.65 GHz instead of 9.8 GHz.

Figure 2 shows photographs of the fabricated prototype and depicts the connection of ground planes by the coaxial connector.

3. RESULTS

Figure 3 compares the measured reflection coefficient with that obtained from the time-domain solver of CST Microwave Studio. Good agreement is observed with a minimum measured return loss of 9 dB in the three bands that range from 4.23 to 4.62 GHz, 6.6 to 8.175 GHz, and 9.39 to 10.7 GHz.

Figure 4 depicts the simulated co- and cross-polarized field components E_θ and E_ϕ (cf., Fig. 1), respectively, with a probe located in the far field at $\theta = 90°$ and $\phi = 90°$. The copolarized fields are predominant in the pass-bands and similar to the cross-polarized ones in the stop-bands.

For the same scenario, Figure 5 shows the simulated group delay performances of the two polarizations. As the signal is dominated by the copolarized field, the group delay in copolarized direction is the main focus. Its variation is less than 80 ps in the three pass-bands.

Figures 6–10 compare the simulated and measured normalized radiation patterns for frequencies of 4.3, 5, 7, 9, and 10 GHz. The first two plots in each figure [(a) and (b)] are the *H*-

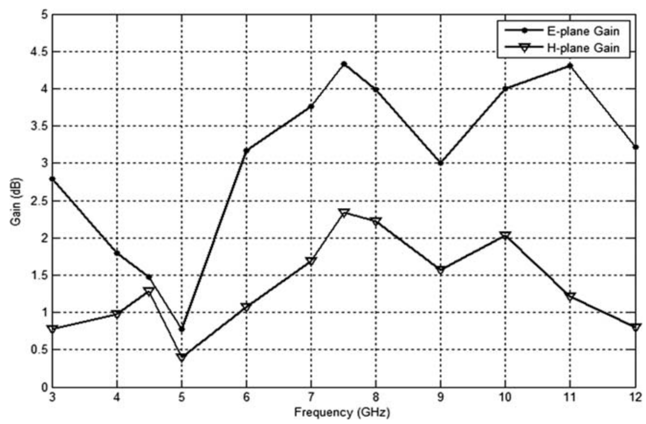

Figure 11 Simulated gain performances of UWB antenna with SIW resonators: maximum gain in the *E*-plane ($\Phi = 90°$) and *H*-plane ($\Theta = 90°$)

plane, and the last two [(c) and (d)] are the *E*-plane radiation patterns. In addition, the plots on the left side of each figure [(a) and (c)] are the copolarized, those on the right side [(b) and (d)] the cross-polarized radiation patterns. Figures 6, 8, and 10 show the radiation patterns in the pass-bands, whereas those in Figures 7 and 9 are in the stop-bands.

Good agreement between simulations and measurements is demonstrated. It is observed that in the pass-bands, the copolarized radiation levels are at least 10 dB above the cross-polarized ones. In the stop-bands, the copolarized fields have similar low power levels as the cross-polarized ones. This is in reasonable agreement with the amplitude responses as shown in Figure 4.

Figure 11 depicts the simulated gain performance of the UWB antenna with SIW resonators. (Note that calibrated gain could not be measured.) Because the direction of maximum radiation changes with frequency according to Figures 6–10, two gain curves are presented in Figure 11: the *E*-plane plot is the maximum gain obtained when varying angle θ at $\phi = 90°$, that is, the *yz* plane in Figure 1. The *H*-plane plot is the maximum gain when varying angle ϕ in the *H*-plane at $\theta = 90°$, that is, the *xy* plane in Figure 1. It is observed that both *E*-plane and *H*-plane gains have notches at the stop-band frequencies of around 5 and 9 GHz.

4. CONCLUSION

Using SIW cavities in printed-circuit UWB antennas is a viable option to create dual-stop-bands for the purpose of alleviating signal interference in UWB systems. Because a half-wavelength SIW resonator designed for the 6 GHz band will produce a second notch within the UWB due to the next harmonic resonance, three pass-bands separated by two stop-bands are produced. The design that uses a CPW-fed UWB antenna with two symmetric SIW resonators is experimentally verified with respect to input reflection coefficient and pass- and stop-band radiation patterns. In the three pass-bands, amplitude responses, group delays, and gains are reasonable and compared well with other printed-circuit UWB antennas. The pass-band return loss is significantly better than a previous attempt to utilize an SIW cavity within a UWB antenna setting.

REFERENCES

1. J. Liang, C.C. Chiau, X. Chen, and C.G. Parini, Study of a printed circular disc monopole antenna for UWB systems, IEEE Trans Antennas Propag 53 (2005), 3500–3504.
2. C.-C. Lin, Y.-C. Kan, L.-C. Kuo, and H.-R. Chuang, A planar triangular monopole antenna for UWB communication, IEEE Microwave Wireless Compon Lett 15 (2005), 624–626.
3. K. Rambabu, M. Alam, J. Bornemann, and M.A. Stuchly, Compact wideband dual-polarized microstrip patch antenna, In: IEEE Antennas and Propagation Society (AP-S) International Symposium Digest, Monterey, CA, June 2004, pp. 1955–1958.
4. M. Mokhtaari and J. Bornemann, Printed-circuit antennas for 3–30 GHz and 3–60 GHz UWB applications, In: Proceedings of Asia-Pacific Microwave Conference, Yokohama, Japan, December 2010, pp. 1922–1925.
5. T.-G. Ma and C.-H. Tseng, An ultrawideband coplanar waveguide-fed tapered ring slot antenna, IEEE Trans Antennas Propag 54 (2006), 1105–1110.
6. R. Chair, A.A. Kishk, and K.F. Lee, Ultrawide-band coplanar waveguide-fed rectangular slot antenna, IEEE Antennas Wireless Propag Lett 3 (2004), 227–229.
7. J.I. Kim and Y. Jee, Design of ultrawideband coplanar waveguide-fed LI-shape planar monopole antennas, IEEE Antennas Wireless Propag Lett 6 (2007), 383–387.
8. K. Kiminami, A. Hirata, and T. Shiozawa, Double-sided printed bow-tie antenna for UWB communications, IEEE Antennas Wireless Propag Lett 3 (2004), 152–153.
9. Q.-X. Chu and Y.-Y. Yang, A compact CPW-fed planar ultra-wideband antenna with a frequency notch characteristic, In: Proceedings of Asia-Pacific Microwave Conference, Bangkok, Thailand, December 2007, pp. 1–4.
10. S.-H. Choi, H.-J. Lee, and J.-K. Kim, Design of a ultra-wideband antenna with band notch characteristic, In: IEEE Antennas and Propagation Society (AP-S) International Symposium Digest, San Diego, CA, July 2008, pp. 1–4.
11. H.M. Jafari, M.J. Deen, S. Hranilovic, and N.K. Nikolova, Slot antenna for ultra-wideband applications, In: IEEE Antennas and Propagation Society (AP-S) International Symposium Digest, Albuquerque, NM, July 2006, pp. 1107–1110.
12. J. Liu, K.P. Esselle, and S. Zhong, Creating multiple band notches in an extremely wideband printed monopole antenna, In: Proceedings of Asia-Pacific Microwave Conference, Yokohama, Japan, December 2010, pp. 2220–2223.
13. Q. Wang, A coplanar waveguide UWB antenna with notch filter, Master of Applied Science Thesis, University of Victoria, Victoria, BC, Canada, June 2013.
14. F. Taringou, D. Dousset, J. Bornemann, and K. Wu, Broadband CPW feed for millimeter-wave SIW-based antipodal linearly tapered slot antennas, IEEE Trans Antennas Propag 61 (2013), 1756–1762.
15. W. Hong, Y. Zhang, C. Yu, Z.Q. Kuai, J.Y. Zhou, Z.Q. Wang, and Y. Dong, Compact ultra-wideband antenna with multiple stop bands, In: Proceedings of International Workshop Antenna Technology (iWAT), Chiba, Japan, March 2008, pp. 32–34.
16. L. Yan, W. Hong, G. Hua, J. Chen, K. Wu, and T.J. Cui, Simulation and experiment on SIW slot array antennas, IEEE Microwave Wireless Compon Lett 14 (2004), 446–448.
17. D. Deslandes and K. Wu, Accurate modeling, wave mechanisms, and design considerations of a substrate integrated waveguide, IEEE Trans Microwave Theory Tech 54 (2006), 2516–2526.

COMPARISON OF PERFORMANCE OF COMPACT RING PRINTED MONOPOLE AND LOOP ANTENNAS FOR WIRELESS-IMPLANTABLE BODY AREA NETWORK APPLICATIONS

Nur Hidayah Ramli,[1] Muhammad Ramlee Kamarudin,[1] Ezla Najwa Ahyat,[1] Nor Asmawati Samsuri,[2] Nor Hisham H. Khamis,[2] A. Y. Abdulrahman,[1] and Muhammad Fitri Ayob[3]
[1] Wireless Communication Centre (WCC), Faculty of Electrical Engineering, Universiti Teknologi Malaysia, UTM, Skudai, Johor 81310, Malaysia; Corresponding author: ramlee@fke.utm.my
[2] Department of Radio Communication Engineering, Faculty of Electrical Engineering, Universiti Teknologi Malaysia, UTM, Skudai, Johor 81310, Malaysia
[3] Department of Electronic and Communication, College of Engineering, Universiti Tenaga Nasional, Kajang, Selangor 43000, Malaysia

Received 13 September 2013

ABSTRACT: *Human bodies have a variety of tissues and organs, and so it needs to be characterized as a radio-wave propagation medium to create a reliable wireless communication link. The radiation characteristics of printed monopole antenna and printed loop antenna for wireless-implantable body area network (WiBAN) applications are presented in this article. The two antennas are submerged into canola oil to mimic an implanted antenna in the human tissue. The tissue is considered a lossy environment and hence, it adversely degrades radiation characteristics of both antennas. Therefore, the RF transmission attenuation, dB*